Sea spray aerosol as a unique source of ice nucleating particles

Paul J. DeMott[a,1], Thomas C. J. Hill[a], Christina S. McCluskey[a], Kimberly A. Prather[b,c], Douglas B. Collins[b], Ryan C. Sullivan[d], Matthew J. Ruppel[b,2], Ryan H. Mason[e], Victoria E. Irish[e], Taehyoung Lee[f], Chung Yeon Hwang[g], Tae Siek Rhee[g], Jefferson R. Snider[h], Gavin R. McMeeking[i], Suresh Dhaniyala[j], Ernie R. Lewis[k], Jeremy J. B. Wentzell[l], Jonathan Abbatt[m], Christopher Lee[b], Camille M. Sultana[b], Andrew P. Ault[n,o], Jessica L. Axson[o], Myrelis Diaz Martinez[p], Ingrid Venero[p], Gilmarie Santos-Figueroa[p], M. Dale Stokes[c], Grant B. Deane[c], Olga L. Mayol-Bracero[p], Vicki H. Grassian[q], Timothy H. Bertram[r], Allan K. Bertram[e], Bruce F. Moffett[s], and Gary D. Franc[t,3]

[a]Department of Atmospheric Science, Colorado State University, Fort Collins, CO 80523-1371; [b]Department of Chemistry and Biochemistry, University of California, San Diego, La Jolla, CA 92093; [c]Scripps Institution of Oceanography, University of California, San Diego, La Jolla, CA 92093; [d]Center for Atmospheric Particle Studies, Carnegie Mellon University, Pittsburgh, PA 15213; [e]Department of Chemistry, University of British Columbia, Vancouver, BC, Canada V6T1Z1; [f]Department of Environmental Science, Hankuk University of Foreign Studies, Yongin 449791, South Korea; [g]Korea Polar Research Institute, Yeonsu-gu, Incheon 406840, South Korea; [h]Department of Atmospheric Science, University of Wyoming, Laramie, WY 82071; [i]Handix Scientific, Boulder, CO 80301; [j]Department of Mechanical and Aeronautical Engineering, Clarkson University, Potsdam, NY 13699; [k]Environmental and Climate Sciences Department, Brookhaven National Laboratory, Upton, NY 11973; [l]Air Quality Processes Research Section, Environment Canada, Toronto, ON, Canada M3H 5T4; [m]Department of Chemistry, University of Toronto, Toronto, ON, Canada M5S 3H6; [n]Department of Chemistry, University of Michigan, Ann Arbor, MI 48109; [o]Department of Environmental Health Sciences, University of Michigan, Ann Arbor, MI 48109; [p]Department of Environmental Science, University of Puerto Rico, San Juan, PR 00931; [q]Department of Chemistry, University of Iowa, Iowa City, IA 52242; [r]Department of Chemistry, University of Wisconsin, Madison, WI 53706; [s]Ocean Lab, Fishguard Harbour, Goodwick, Pembrokeshire SA64 0DE, United Kingdom; and [t]Department of Plant Sciences, University of Wyoming, Laramie, WY 82071

Ice nucleating particles (INPs) are vital for ice initiation in, and precipitation from, mixed-phase clouds. A source of INPs from oceans within sea spray aerosol (SSA) emissions has been suggested in previous studies but remained unconfirmed. Here, we show that INPs are emitted using real wave breaking in a laboratory flume to produce SSA. The number concentrations of INPs from laboratory-generated SSA, when normalized to typical total aerosol number concentrations in the marine boundary layer, agree well with measurements from diverse regions over the oceans. Data in the present study are also in accord with previously published INP measurements made over remote ocean regions. INP number concentrations active within liquid water droplets increase exponentially in number with a decrease in temperature below 0 °C, averaging an order of magnitude increase per 5 °C interval. The plausibility of a strong increase in SSA INP emissions in association with phytoplankton blooms is also shown in laboratory simulations. Nevertheless, INP number concentrations, or active site densities approximated using "dry" geometric SSA surface areas, are a few orders of magnitude lower than corresponding concentrations or site densities in the surface boundary layer over continental regions. These findings have important implications for cloud radiative forcing and precipitation within low-level and midlevel marine clouds unaffected by continental INP sources, such as may occur over the Southern Ocean.

marine aerosols | ice nucleation | clouds

Cloud particles form on atmospheric aerosols, and through this action aerosol particles may impact cloud properties and climate via so-called aerosol indirect effects (1). In clouds that are not cold enough for homogeneous freezing of condensed liquid water to occur (below approximately −38 °C), the first initiation of ice requires the presence of ice nucleating particles (INPs) (2), a select subgroup that may represent 1 in 10^6 or fewer of all aerosol particles (3). INPs are thus extremely important to the Earth's radiative balance and to precipitation in regions dominated by cold clouds; their impacts may be regionally distinct due to differences in aerosol sources and their variability. INPs affect all mixed-phase (ice and liquid coexisting) clouds, and all-ice clouds (e.g., cirrus) below −38 °C, where their action may permit cloud formation at lower supersaturations or warmer temperatures than for homogeneous freezing acting alone (4, 5).

Terrestrial sources of INPs have received much past attention. In particular, the action of both mineral (4, 6–8) and arable soil

dust (9–11) particles as continental sources of INPs is well documented, and recent studies suggest that perturbations of the soil and plant surfaces leads to the release of biological organisms that can serve as INPs (12–14). Other recent publications also document sources of INPs from biomass burning (15, 16) and others have indicated potential contributions of anthropogenic pollution particles (17, 18) as INPs.

The relative importance of oceans as a source of INPs, presumably as a component within the sea spray aerosol (SSA), in comparison with terrestrial sources, remains an open question (3, 19–21). Oceans cover the greatest percentage of the Earth's surface area and dominate in the Southern Hemisphere (SH). INPs of different types have been found in seawater, and variable production and occasional hot spots have been suggested based on past measurements of air over oceans (20, 22–25), with a common inference that specially active or abundant sources are from oceanic biological microorganisms, or are mediated by the products of their life processes (20, 23, 26–28). For example, relation between INP emissions and emitted primary organic material in SSA has been proposed and used in modeling studies (20, 28). Nevertheless, it is notable in the study by Burrows et al. (20) that mineral dust transports were predicted to dominate INP populations over broad global regions dominated by land masses or in dust belts,

whereas high INP emissions from marine sources required a constraining assumption that past INP measurements over remote marine regions, such as those by Bigg (22), likely represent underestimates.

The primary reason to document the production of INPs from oceans is that, over vast oceanic regions, sea spray-released INPs may help control the typical liquid/ice phase structure, and thus radiative properties, of clouds over large regions. Emissions are of course only one part of such a hypothesis, atmospheric structure, aerosol transports, and cloud dynamics being the other factors determining which INPs reach and impact supercooled clouds. Nevertheless, global models consistently underestimate the outgoing (i.e., reflected) short-wave solar radiation in regions dominated by oceans, especially in the SH (29). This underestimation has been attributed to simulating too few and too short-lived clouds, in conflict with the persistent and deeply supercooled clouds that have been observed in satellite retrievals (30, 31). Although model parameterizations, such as those governing planetary boundary layer turbulence and moist convection, can explain some portion of cloud biases in SH midlatitudes (32), a microphysical explanation based around the potential role of a scarcity of INPs over these regions deserves consideration.

In situ data provide some basis for the concept that INP numbers matter, particularly over Southern Ocean regions. This evidence is from polarization lidar measurements indicating a lower ice phase transition temperature, by up to 10 °C, over Southern Ocean regions in comparison with Northern Hemisphere ocean regions nearer to continents (33). Aircraft measurements are limited, but often support low primary ice crystal concentrations (<0.1 L^{-1} at T greater than −20 °C) and other factors that may limit the occurrence of secondary ice crystal generation at greater than −10 °C in these regions (via processes that require preexisting ice crystals formed by primary ice nucleation) (34–36). A consequence is a likely misrepresentation of ice concentrations using numerical model parameterizations based largely on Northern Hemisphere data (36).

Because it is not always possible to determine sources of particles in the ambient marine boundary layer (MBL), studies involving the isolation and characterization of sea spray particles in laboratory settings are needed. The current study uses laboratory systems for simulation of SSA emissions at the Center for Aerosol Impacts on Climate and the Environment (CAICE) (37–39) to investigate INP number concentrations produced from fresh SSA, and compares these data with INP number concentration measurements made on aerosols collected from the MBL at a variety of locations.

Results and Discussion

The INP number concentration datasets are summarized in Fig. 1 A and B. Most laboratory and ambient MBL measurements are given in Fig. 1A, and these are supplemented (Fig. 1B) with historical measurements over oceans, continental boundary layer measurements, and off-line laboratory measurements following the peak of a phytoplankton bloom. Locations and details of ambient measurements are given in *Materials and Methods*, with additional details in *SI Materials and Methods*. Two methods were used in the laboratory to produce SSA particles, continuous breaking waves in the CAICE wave channel or plunging water sheets in a marine aerosol reference tank (MART). Normalized particle size distributions produced by these two methods have been shown to be similar (37–39). Thus, to account for the fact that SSA numbers generated in MART studies are higher (up to 1,000 cm^{-3}) in comparison with the wave channel (~175 cm^{-3}) or natural, unpolluted marine boundary layer values of 50–200 cm^{-3} at the accumulation mode sizes generated in these studies (40), the MART INP data have been normalized to wave channel particle number concentrations through use of the ratio of wave channel to MART total particle number concentrations. INP data are from an on-line and two off-line sampling techniques for INPs, as described in *Materials and Methods*; although representing different sample volumes, they show close agreement over their temperature ranges of overlap (Fig. S1). There is excellent general correspondence between the laboratory and ambient datasets, with
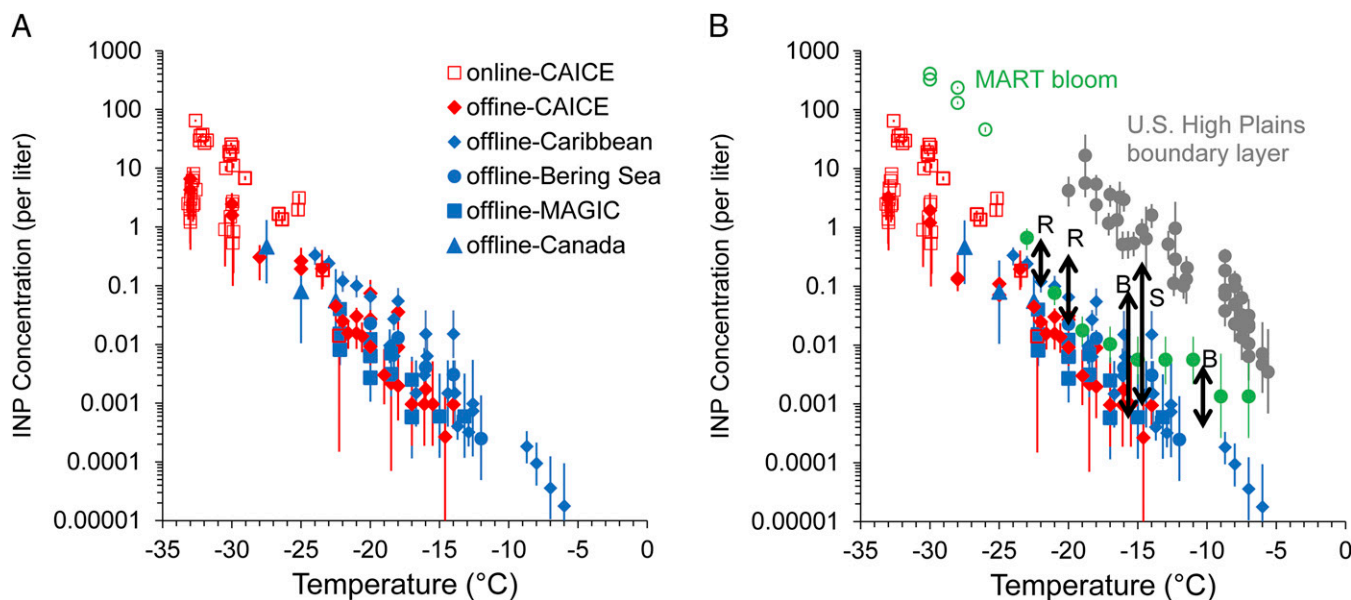

Fig. 1. Assembly of data on INP number concentrations from sea spray particles in the laboratory (red) and for ambient marine boundary layer particles (blue), and differentiated between on-line (open symbols) or off-line (filled symbols) measurements (A and B). Laboratory data are normalized to total particle concentrations of 150 cm^{-3}. Locations/projects are indicated in each case. In B, additional data are included from a day (January 27) following the peak of the MART phytoplankton bloom in January 2013 (green), and for continental boundary layer measurements (gray) (40). Also shown by solid arrows are the ranges of measured INP concentrations in other historical measurements over the Southern Ocean by Bigg (B) (22), from the Gulf of Mexico by Rosinski et al. (R) (24), and from off the east coast of Nova Scotia by Schnell (S) (25). Error bars on data points are discussed in the text.

modestly higher INP number concentrations in the ambient samples. Whereas all of the ambient data are via off-line methods, and there is not complete overlap of the full mixed-phase cloud temperature range, the INP temperature spectrum of number concentrations shows nearly exponentially increasing values as temperatures decrease from −5 °C to below −30 °C, with an order of magnitude increase per ∼5 °C decrease in temperature (Fig. 1*A*).

The SSA INP number concentrations measured in this study are shown to be within the range of INP concentrations measured in some previous studies over oceans (Fig. 1*B*) and are most consistent with the range of values measured at −15 °C more than 40 y previous by Bigg over the Southern Ocean (22). Schnell (25) noted clear instances of continental air influence during portions of that cruise east of Nova Scotia. Fig. 1*B* also shows that INP number concentrations measured for SSA in this study are up to three orders of magnitude lower than have been measured for aerosols present at the surface over the High Plains region of the United States during a late summer and early fall period (41). Continental boundary layer total particle concentrations are usually much higher than over oceans, and the sources of INP can be manifold. Particularly relevant in the contrast of typical boundary layer INP concentrations shown at temperatures warmer than −20 °C in Fig. 1*B* are INPs of plant and soil biological origins. These types may vary by ecosystem, but even INP number concentrations measured in a forest ecosystem (14) exceed those of SSA INPs in Fig. 1 by one to two orders of magnitude at temperatures warmer than −20 °C. Thus, we believe that the differences between land and ocean-sourced INPs shown in Fig. 1*B* are robust.

A MART experiment to explore the role of phytoplankton blooms on production of INPs is shown in Fig. 2. The bloom in this experiment was artificially initiated and enhanced to high chlorophyll *a* (Chl *a*) concentrations through serial additions of phytoplankton grown in smaller beakers. However, the salient information sought in this case was to determine whether INP number concentrations could be affected by a strong Chl *a* perturbation. A limiting factor in data collection for these experiments was the need not to perturb the seawater system until the onset of bloom conditions was noted. Only a single, short sampling period [continuous flow diffusion chamber (CFDC) data at −30 °C] was allowed before sampling on January 25. Ice nucleation measurements were also limited by scheduling through January 30, preventing measurements through bloom death. Nevertheless, notable in Fig. 2 is the strong enhancement of INP numbers by up to 50 times in comparison with fresh seawater cases at −26 and −30 °C, in kind with similar enhancements to the Chl *a* concentration. Enhancement was not observed uniformly across different temperature regimes (Fig. 2), nor in comparison with fresh seawater
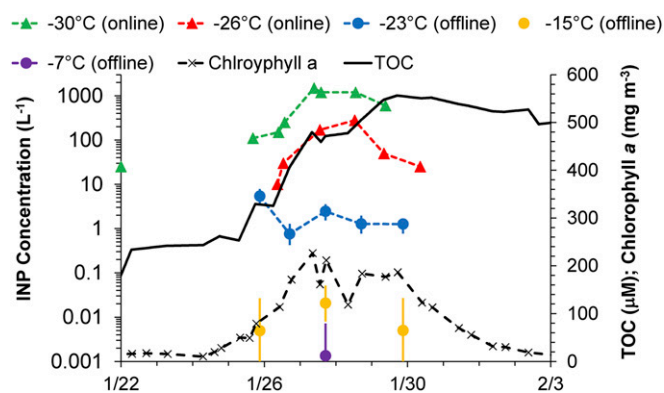
cases (Fig. 1*B*), suggesting the involvement of different INP elements active at different temperatures. Although significant increases in INP number concentrations were not measured at −23 or −15 °C following the peak of Chl *a* values, appearance of measurable INP number concentrations at warmer than −15 °C occurred on January 27, as demonstrated in Fig. S2 and highlighted in Fig. 1*B*. Although it remains to be shown that such enhancements regularly occur also for blooms at Chl *a* concentrations more realistic for the ocean, these results imply a potentially strong sensitivity of INP production from SSA that is linked to changes in chemistry induced by biological processes in seawater. The involvement and definition of specific INP compositions remains to be fully explored. Inferences on the organic and likely biological nature of INP compositions that are enhanced at the warmest temperatures during blooms have been provided in another recent study (42). Furthermore, enhancements in INP number concentrations from sea spray under high Chl *a* provide indirect evidence that INP composition is indeed linked to some compartments of organic matter. Nevertheless, high total organic carbon (TOC) levels after the bloom peak occurred in concert with a degradation of INP enrichments at lower temperatures, similar to some previous observations (37). Enrichment in INP number concentrations when sintered glass filters were used for bubble generation (*Materials and Methods*), a method known to artificially enhance organic carbon content in SSA at all sizes (38), also supports a likely dominance of organic INPs in SSA. Those results also support that INP units extend to small sizes in seawater, as recently confirmed by others (28).

Atmospheric Implications. Although the results in Fig. 1 already demonstrate an expected difference of the contribution of INPs to clouds over oceans versus land, a more quantitative framework that permits comparison of different source aerosols on the basis of total aerosol surface area is introduced, which may have applications in numerical models. For this purpose, we calculated the surface active site density parameter, n_s, with units per surface area, per square centimeter in this case. This parameter is commonly used for comparing the potency of different INPs (8, 43). These calculations tacitly assume that SSA INPs can potentially be represented as a single and unique INP type, much as mineral and soil dust INPs have been represented in previous studies. Although the use of the total SSA surface area may be a gross simplification because the material that contains the INP may not comprise the entire particle (e.g., if organic coatings are the source), this assumption offers a fair basis for comparison with these other specific terrestrial aerosol types. Results of such a computation on the basis of dry aerosol surface area and an assumption of sphericity for all laboratory and field SSA particles (*SI Materials and Methods*) are shown in Fig. 3. For comparison, n_s curves defined for different specific land surface dust sources in laboratory studies are also presented. Values of n_s reported for soil dust sources are typically two to three orders of magnitude greater than values from SSA. We also note that n_s values derived by others from previous experimental studies for marine diatoms (27, 43) are in close agreement with the SSA INP data in Fig. 3. This result is somewhat surprising, given that the diameters of aerosols sampled at temperatures less than −23 °C with the continuous flow diffusion chamber were limited below 2.5 μm in the current study, whereas most diatoms are >2 μm in diameter. Recent findings indicating that diatom exudates contain smaller ice nucleation entities (28) provide a potential explanation for this correspondence, although sufficient information does not yet exist to confirm this numerically. Values of n_s determined from laboratory-generated particles were lower than those from ambient particles, possibly because of the enhanced surface area of nascent laboratory SSA at dry diameters greater than ∼1 μm, as atmospheric microphysical and cloud processing may naturally reduce concentrations and surface

Fig. 2. Time series of INP number concentrations, Chl *a*, and total organic carbon (TOC) at selected temperatures during the MART bloom experiment in January 2013.
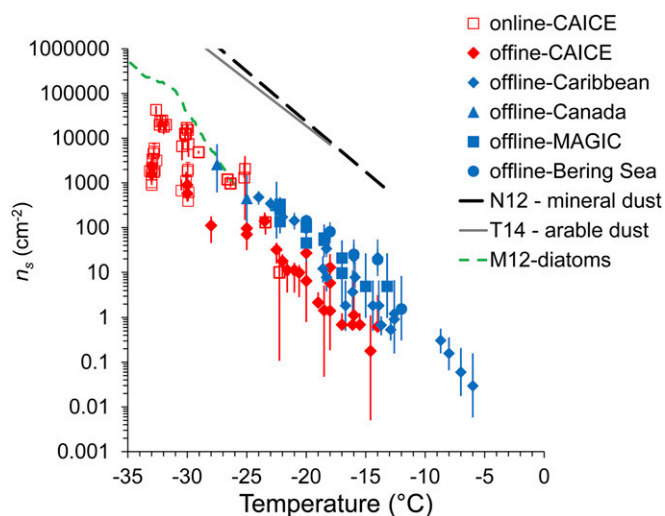
Fig. 3. Surface active site density, n_s, for all data shown in Fig. 1A. Average n_s values for mineral dust (8), arable soil dust (11), and diatoms (43) are shown for comparison with the calculated values.

areas of ambient particles at these sizes (44). Fig. 4 shows similar ambient aerosol size distributions in the Pacific Ocean near Hawaii during one of the Marine ARM (Atmospheric Radiation Measurement) GPCI (Global Energy and Water Cycle Experiment Cloud System Study Pacific Cross-section Intercomparison) Investigations of Clouds (MAGIC) filter samples, and during two periods of the Canadian Arctic sampling [Network on Climate and Aerosols: Addressing Key Uncertainties in Remote Canadian Environments (NETCARE)], indicating the relative absence of the larger diameter mode in number and surface area. The inherent size distribution of INPs present is not known in the laboratory and ambient samples in this paper. However, it is possible that a disproportionate amount of sea salt at dry diameters larger than 1 μm in the nascent laboratory case (37) compared with the ambient marine samples is artificially lowering n_s, because sea salt is not known to be ice nucleation active in the temperature regime studied. We also note that our assumption of efficient transfer of particles to the

CAICE off-line filter samples up to sizes of 2.5 μm that was not directly validated (*Materials and Methods*) encompasses three times the surface area present in the submicron size range alone. Thus, n_s values from those ice spectrometer (IS) filter samples should be considered as conservative lower estimates.

Materials and Methods

Laboratory SSA Particle Generation from Seawater. On-line and off-line INP measurements conducted at CAICE facilities at the University of California, San Diego, and Scripps Institution of Oceanography (SIO) involved sampling of SSA produced via breaking waves in a 33-m-long, 0.6-m-deep, 9,900-L volume glass-walled wave channel (37, 38) and plunging waterfalls in a MART (39). These methods have been shown to be consistent with each other in producing a broad nascent SSA size distribution due to bubble bursting, in contrast to the production of SSA particles by forcing air through sintered glass filters within seawater samples (37). In preliminary tests, we determined that use of plunging waterfalls and wave breaking in a laboratory setting produced consistent and comparable INP number concentrations measurements (Fig. S3), whereas use of glass frits to generate bubbles produced more INPs. These differences highlight the inaccuracies that can be introduced by not realistically simulating the natural sea spray production process. Whether these additional INPs are from an enhanced fresh particle size mode at geometric dry diameter less than 0.1 μm or from the enhanced organic matter known to be placed into SSA (especially at dry diameters greater than 0.5 μm) when using sintered glass filters (38) is worth further study.

In experiments used for this study, the wave channel or MART was filled with natural, coastal seawater from 275 m offshore and ~4 m below the low-tide line at the SIO Pier (La Jolla, CA) (32°52.00′ N, 117°15.40′ W). Reported data (*Supporting Information* data compilation and Dataset S1) were collected during periods of wave breaking of relatively fresh seawater, usually before nutrient addition for stimulation of phytoplankton blooms. Similarly, most data reported for MART experiments were collected during the period before bloom conditions, except as noted. Seawater Chl *a* concentrations were measured in real time using a WET Labs ECO Triplet customizable fluorimeter operating at 695 nm. Aerosol number and surface area size distribution measurements were made following previously documented methods that involve drying particles to <15% relative humidity, and use simplifying assumptions to connect electrical mobility and aerodynamic sizing measurements to define spherical equivalent particles up to a diameter of 20 μm (39).

Ambient Marine Aerosol Samples. Field samples for analysis of INP number concentrations per volume of air using off-line immersion freezing methods came from a variety of studies on aircraft, ships, and island sites under marine airflow. The siting of measurements is detailed in *SI Materials and Methods* (Figs. S4–S7). Larger sample volumes of particles were collected from air through
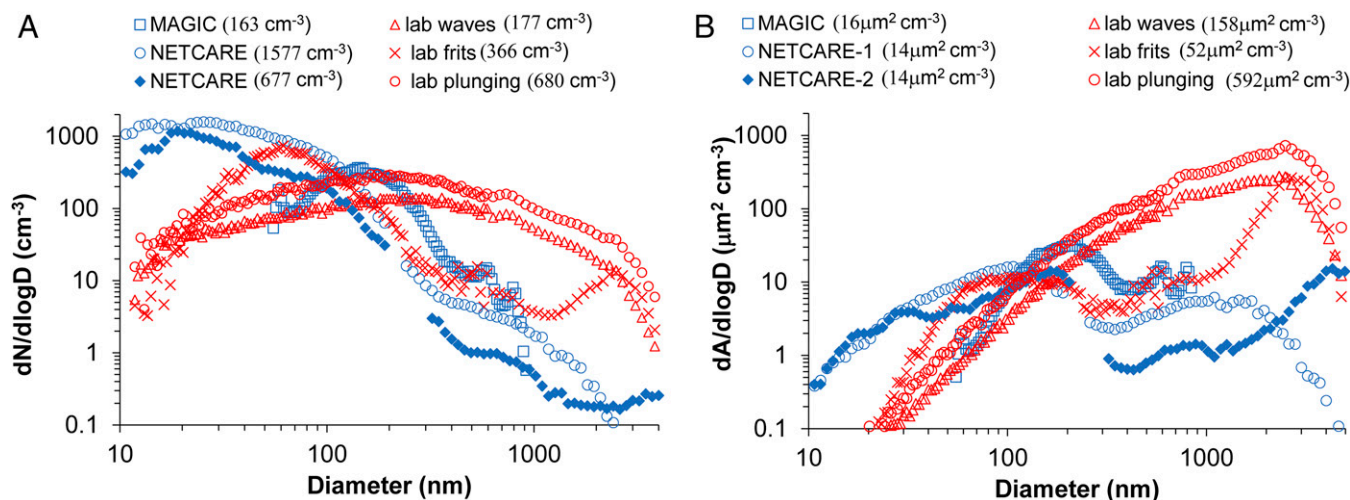

Fig. 4. Size distributions of concentrations of (A) aerosol number and (B) surface area for three laboratory particle generation methods (in red) (38, 39, 44), compared with ambient aerosol size distributions (in blue) measured by the ultrahigh-sensitivity aerosol spectrometer instrument during the open ocean IS filter sampling period east of Hawaii during the MAGIC study and two sampling periods during the 2014 NETCARE program. Total integrated particle number and surface area for each distribution is shown in parentheses in the legend.

polycarbonate filters or onto glass substrates for the various off-line measurement methods detailed below. Filters were collected for off-line processing during National Science Foundation (NSF)/National Center for Atmospheric Research (NCAR) C-130 aircraft flights for the Ice in Clouds–Tropical (ICE-T) study, based from St. Croix, US Virgin Islands (45, 46); only filters collected in the MBL have been included. During this study, filter collections were also made at two sites in Puerto Rico, one a northeastern coastal site at Cape San Juan [66 m above mean sea level (MSL)] and one at a mountaintop research station at Pico del Este (1,051 m above MSL, typically the top of the MBL in this region). Ship-based filter collections used here occurred during two campaigns. The first, the Ship-borne Pole-to-Pole (SHIPPO) experiment was operated on the Korea Polar Research Institute R/V *Araon* during Summer 2012. This cruise followed a path from Incheon, South Korea, to Nome, Alaska, with filter samples collected over a 9-d period. A representative sample from the Bering Sea is used in this study. Other filter collections were made onboard the Horizon *Spirit* container ship during Los Angeles to Honolulu and return cruises as part of the MAGIC (47) study in Summer 2013, supported and undertaken by the ARM Climate Research Facility of the US Department of Energy. Finally, size-selective collections of aerosols onto glass coverslips were made onboard the icebreaker CGSS *Amundsen* in the Canadian Arctic Archipelago during the NETCARE project in Summer 2014. Additional details regarding filter and coverslip collections are detailed in the section describing off-line immersion freezing measurements.

On-Line INP Measurements. On-line INP number concentration measurements were performed during MART and wave channel studies using two physically identical CFDCs (48–50). At the heart of these instruments is a chamber composed of concentric cylindrical copper walls that have been chemically treated to allow them to become wetted by liquid water so that a uniform ice surface is solidly frozen to the walls. The two walls are separated by 1.12 cm and are typically coated to an ice thickness of 0.015 cm. An aerosol lamina representing 15%, or 1.5 L·min^{-1}, of the total volume flow of 10 L·min^{-1} is delivered to a central ring between the ice plates, surrounded by recirculating particle-free sheath flows. The chamber is divided into two sections vertically, separated by a Delrin collar. A temperature gradient between the colder (inner) and warmer (outer) ice walls in the upper region is achieved by circulating refrigerant through separate coils that are heat sunk to the wall surfaces that are not iced to maintain approximately constant temperatures along the upper 50-cm sections of each wall. The differential cooling between the walls creates an ice supersaturated field in the flowing air, and the temperature and humidity conditions at any point can be calculated. Ice crystals forming on INPs in the upper growth region of the chamber enter a lower 30-cm section where the two walls are controlled equivalently to the original cold (inner) wall temperature to promote evaporation of liquid water from droplets and aerosols. This evaporation allows optical detection of ice crystals as the largest particles leaving the chamber.

For this study, water supersaturated conditions (typically water relative humidity equal to 105%) were used to activate cloud droplets on aerosols at temperatures where some proportion could freeze during the several second transit time in the instruments. Aerosol particles at sizes that might confound optical detection of ice crystals are removed upstream of the chamber using dual single-jet impactors set to a cutpoint aerodynamic diameter of 2.4 μm for data retained herein. Ice crystals and aerosols exiting the CFDC at diameters above ~500 nm are counted with an optical particle counter, where the aerosol and ice populations are readily distinguished. All particles with optical diameters >4 μm were assumed to be ice particles. Processing temperature ranged from about −20 to −34 °C. Typical sample periods at constant temperature and supersaturation were 10–30 min long, alternated with periods sampling filtered air to correct for any background frost influences on ice particle counts. Error bars in average INP number concentrations are given by twice the Poisson sampling error for the corrected number of counts obtained in each sampling period. Particle losses in upstream tubing, the aerosol impactor, and the inlet manifold of the CFDC have previously been estimated as 10% for particles with diameter 0.1–0.8 μm (51), and we apply this correction to data for this paper. CFDC sampling was done from air in the headspace of the MART and wave channels, typically from a common manifold used for all aerosol measurements.

Off-Line Immersion-Freezing Methods. Two immersion-freezing methods were used to obtain INP data for particles collected onto substrates, followed by their incorporation into liquid volumes (in different manners) for freezing studies. Each method also involved different collection methods, which varied in the laboratory and field studies, so the freezing methods, sampling protocol, and particulars of calculations required are described separately in order here.

The first freezing method used the CSU IS (41, 52, 53), a device in which an array of liquid aliquots in a temperature-controlled block can be monitored

for freezing as temperature is decreased. Particles are first collected onto filters, and then resuspended in water for distribution into the aliquots.

Particles for IS processing were collected on presterilized 0.2-μm-pore diameter, 47-mm-diameter Nuclepore track-etched polycarbonate membranes (Whatman; GE Healthcare Life Sciences). During ambient air sampling at the ground or on ships, Nalgene sterile filter units (Thermo Scientific) were used to sample onto the open-faced filters for periods ranging from 4 to 54 h (one extreme case) at a typical flow rate of 10 L·min^{-1}. During ship deployments, filters were protected from rain and splash with a shield. On aircraft or during laboratory studies, a presterilized 47-mm in-line stainless-steel filter housing (Pall Corporation) was used to contain the sampling filter and a sterilized 3-μm Nuclepore backing filter. Aircraft filters were collected at 10 L·min^{-1} through a 0.635-cm-inner-diameter copper line that was drawn from a tap angled into the major inlet flow line, which was a 2-inch line entering the aircraft cabin from the exterior aerosol inlet. The exterior inlet was a forward-facing single-stage diffuser nozzle inlet, ingesting air at a flow rate (~700 L·min^{-1}) that was adjusted to be isokinetic at the tip, which was heated to 7 °C to avoid blocking from rime ice accumulating in regions of supercooled cloud water (50). Aircraft filter collection times ranged from 12 to 40 min, sometimes accumulated along multiple level aircraft legs at different altitudes in the boundary layer. Wave channel sampling involved a section of conductive tubing a few meters long coming from the same shared stainless aerosol manifold used for on-line sampling. This manifold was mounted on the top panel of the wave channel, 0.4 m above the water surface and in a position about 1 m beyond the position of the breaking wave. For the MART sampling, air was drawn from a port on the side of the tank, at a level ~15 cm above the breaking bubble surface. Filter sample flow rates were 5 L·min^{-1} from the MART and 10 L·min^{-1} from the wave channel. Particle line losses were not directly investigated during the 2011 studies. Although transfer of all sizes up to 2.5 μm is assumed on the basis of similar line lengths to particle sizing instruments, we may note that surface areas are decreased a factor of 3 for sizes integrated only to 1 μm.

Collection onto the surface or into pores of IS filters in the various sampling scenarios should have exceeded 90% for all particle sizes at the flow rates used on the basis of filter specification and theoretical collection efficiencies (54). Filters and dissembled filter holders were precleaned, separately, by soaking in 10% (vol/vol) H_2O_2 for 10 and 60 min, respectively, followed by three rinses in deionized water (18 MΩ and 0.2-μm-diameter pore filtered). Filters were dried on foil in a particle-free, laminar flow cabinet, as were filter holder components after excess water was removed with a gas duster. After particle collection, filters were stored frozen in sealed sterile Petri dishes until they could be processed.

At the point of IS processing, filters were transferred to sterile, 50-mL Falcon polypropylene tubes (Corning Life Sciences), immersed in 5.0–10.0 mL of 0.2-μm-pore diameter–filtered deionized water, and tumbled for 30 min in a rotator (Roto-Torque; Cole-Palmer) to resuspend particles. Measures of INPs were made on this suspension and on dilutions of it to extend measurements to lower temperatures. This entailed distributing 24–48 aliquots of volume 50–100 μL of suspension into sterile 96-well PCR trays (μCycler; Life Science Products) in the IS. The numbers of wells frozen were counted at 0.5 or 1 °C intervals during cooling at a rate of −1 °C·min^{-1}. Cumulative numbers of INPs per liter of air as a function of temperature [$n_{INPs}(T)$] were estimated using the following formula:

$$n_{INPs}(T) = -\ln\left(\frac{N_u(T)}{N_a}\right)\left(\frac{V_w}{V_a V_s}\right), \qquad \text{[1]}$$

where N_u is the unfrozen number of an initial N_a aliquots, V_w (in milliters) is the volume of purified washing water used to resuspend particles from filters, V_a (in milliliters) is the volume of each aliquot, and V_s is the sample volume (in liters) of air collected. This formula accounts for the fact that each aliquot may hold more INPs than the first one that freezes (55). Correction for any frozen aliquots in the pure water control was made in all cases. Uncertainties are given as binomial sampling confidence intervals (95%) (56).

The second immersion-freezing method involved freezing of droplets grown on substrate-collected particles in a temperature- and humidity-controlled flow cell (57). We will refer to this method as the droplet freezing method, or DFT, herein. Particles from known volumes of air were collected onto hydrophobic glass coverslips (HR3-215; Hampton Research). Droplets were grown in the flow cell by decreasing temperature to 0 °C and passing a humidified flow of He gas over the slides. Droplets were then monitored for freezing, via a coupled optical microscope (Axiolab; Zeiss) with a 4× magnification objective, as temperature was lowered at a constant rate. A CCD camera connected to the optical microscope recorded a digital video while a resistance temperature detector recorded the temperature.

For laboratory wave flume studies, a microorifice uniform deposit impactor (MOUDI) (MSP Corporation) was used to size-select particles for DFT analysis. Multiple MOUDI size stages were used covering 50% cutoff aerodynamic diameter (58) range of 0.32–3.2 μm. Samples were obtained from the same wave channel sampling position as for IS filters, and were then sealed and stored at room temperature until cold stage flow cell measurements were performed at the University of British Columbia.

For DFT processing of the wave channel collections, water was allowed to condense until 65- to 135-μm-diameter water droplets formed on the collected particles. The droplets were then cooled at a rate of −5 °C·min⁻¹ until all were frozen. The method to obtain the INP number concentrations in this case follows a similar basis as for the IS:

$$n_{INPs}(T) = -\ln\left(\frac{N_u(T)}{N_o}\right) N_o \left(\frac{A_{deposit}}{A_{monitored} V_s}\right) f_{nu} f_{ne}, \quad [2]$$

where $N_u(T)$ is the number of unfrozen droplets at temperature T, N_o is the total number of droplets condensed onto the sample, $A_{deposit}$ is the total area of the sample deposit on the hydrophobic glass coverslip, $A_{monitored}$ is the area of the sample monitored in the digital video during the droplet-freezing experiment, V_s is the volume of air sampled by the MOUDI, f_{ne} is a correction factor to account for the uncertainty associated with the number of nucleation events in each experiment (59), and f_{nu} is a correction factor to account for nonuniformity in particle concentration across each MOUDI sample (only a fraction of the entire sample is analyzed) (12, 57). Unlike in the study by Mason et al. (57), substrate holders were not used to position the hydrophobic glass coverslips in a specific location within the MOUDI for wave channel studies, but instead we estimated the positions of the hydrophobic glass coverslips within the MOUDI from the patterns of the aerosol deposits on them. The uncertainty in the INP number concentration takes into account the uncertainty in this position for the wave channel data.

For ship-based coverslip collections during NETCARE, a single-stage impactor (MSP Corporation) was operated with a flow rate of ~10 L·min⁻¹, resulting in collection of particles with aerodynamic diameter >0.18 μm. The impactor was located on the bridge of the ship, and the sampling height was ~15 m above sea level. Sampling collection times were ~20 min. Particles on the hydrophobic glass slides were concentrated into 300 spots due to the design of the nozzle plate used inside the impactor. Typically, 20 spots could be viewed in a given freezing experiment at the magnification used. Condensed droplet sizes were 100–150 μm in diameter, and the DFT flow cell was cooled at a constant rate of −10 °C·min⁻¹ for these samples. For these particular experiments, Eq. **2** for $n_{INPs}(T)$ was modified to the following form:

$$n_{INPs}(T) = -\ln\left(\frac{N_u(T)}{N_d}\right)\left(\frac{300}{V_s}\right), \quad [3]$$

where N_d is the total number of spots of particles in the field of view, which ranged from 16 to 22, $N_u(T)$ in this case is the number of droplets covering spots remaining unfrozen at temperature T, and V_s is again the sampled volume of air, and the factor 300 accounts for observing only N_d spots out of a potential 300 in the freezing experiments. Up to 2% of freezing events occurred when a growing ice crystal came into contact with an unfrozen droplet on the same slide; these events were excluded.

Aerosol Measurements. Measurements of aerosol particle size and number concentration, and total aerosol scattering via nephelometry in MAGIC, were made coincident with INP sampling periods. These measurements, which varied by type for different projects as discussed in *SI Materials and Methods*, served as the basis for computation of total dry aerosol surface area per unit volume (S_{tot} in units of square micrometers per cubic centimeters), used to determine INP surface active site density, n_s (per square centimeter). Computation of n_s followed from the following:

$$n_s(T) = n_{INPs}(T)\left(\frac{10^5}{S_{tot}}\right). \quad [4]$$

The 10^5 factor in Eq. **4** is due to $n_{INPs}(T)$ having units per liter. Surface area measurements are tabulated in Dataset S1, and the measurement basis is provided in each case, while the particular instruments and assumptions, if any, needed to convert measurements to dry particle conditions are given in the *SI Materials and Methods* description for each project.

1. Boucher O, et al. (2013) Clouds and aerosols. *Climate Change 2013: The Physical Science Basis. Contribution of Working Group I to the Fifth Assessment Report of the Intergovernmental Panel on Climate Change*, eds Stocker TF, et al. (Cambridge Univ Press, Cambridge, UK), pp 571–657.
2. Vali G, DeMott PJ, Möhler O, Whale TF (2015) Ice nucleation terminology. *Atmos Chem Phys* 15(18):10263–10270.
3. DeMott PJ, et al. (2010) Predicting global atmospheric ice nuclei distributions and their impacts on climate. *Proc Natl Acad Sci USA* 107(25):11217–11222.
4. DeMott PJ, et al. (2003) Measurements of the concentration and composition of nuclei for cirrus formation. *Proc Natl Acad Sci USA* 100(25):14655–14660.
5. Cziczo DJ, et al. (2013) Clarifying the dominant sources and mechanisms of cirrus cloud formation. *Science* 340(6138):1320–1324.
6. DeMott PJ, et al. (2003) African dust aerosols as atmospheric ice nuclei. *Geophys Res Lett* 30(14):1732.
7. Isono K, Komabayasi M, Ono A (1959) The nature and the origin of ice nuclei in the atmosphere. *J Meteorol Soc Jpn* 37(6):211–233.
8. Niemand M, et al. (2012) Parameterization of immersion freezing on mineral dust particles: An application in a regional scale model. *J Atmos Sci* 69(10):3077–3092.
9. Conen F, Morris CE, Leifeld J, Yakutin MV, Alewell C (2011) Biological residues define the ice nucleation properties of soil dust. *Atmos Chem Phys* 11(18):9643–9648.
10. O'Sullivan D, et al. (2014) Ice nucleation by fertile soil dusts: Relative importance of mineral and biogenic components. *Atmos Chem Phys* 14(4):1853–1867.
11. Tobo Y, et al. (2014) Organic matter matters for ice nuclei of agricultural soil origin. *Atmos Chem Phys* 14(16):8521–8531.
12. Huffman JA, et al. (2013) High concentrations of biological aerosol particles and ice nuclei during and after rain. *Atmos Chem Phys* 13(13):6151–6164.
13. Prenni AJ, et al. (2013) The impact of rain on ice nuclei populations. *Geophys Res Lett* 40(1):227–231.
14. Tobo Y, et al. (2013) Biological aerosol particles as a key determinant of ice nuclei populations in a forest ecosystem. *J Geophys Res Atmos* 118(17):10100–10110.

15. Prenni AJ, et al. (2012) Biomass burning as a potential source for atmospheric ice nuclei: Western wildfires and prescribed burns. *Geophys Res Lett* 39(11):L11805.
16. McCluskey CS, et al. (2014) Characteristics of atmospheric ice nucleating particles associated with biomass burning in the US: Prescribed burns and wildfires. *J Geophys Res Atmos* 119(17):10458–10470.
17. Wang BB, et al. (2012) Heterogeneous ice nucleation and water uptake by field-collected atmospheric particles below 273 K. *J Geophys Res Atmos* 117(D21):D00V19.
18. Knopf DA, et al. (2014) Microspectroscopic imaging and characterization of individually identified ice nucleating particles from a case field study. *J Geophys Res Atmos* 119(17):10365–10381.
19. Creamean JM, et al. (2013) Dust and biological aerosols from the Sahara and Asia influence precipitation in the western U.S. *Science* 339(6127):1572–1578.
20. Burrows SM, Hoose C, Pöschl U, Lawrence MG (2013) Ice nuclei in marine air: Bioparticles or dust? *Atmos Chem Phys* 13(1):245–267.
21. Rosenfeld DR, et al. (2013) The common occurrence of highly supercooled drizzle and rain near the coastal regions of the western United States. *J Geophys Res Atmos* 118(17):9819–9833.
22. Bigg EK (1973) Ice nucleus concentrations in remote areas. *J Atmos Sci* 30(6):1153–1157.
23. Rosinski J, Haagenson PL, Nagamoto CT, Parungo F (1987) Nature of ice-forming nuclei in marine air masses. *J Aerosol Sci* 18(3):291–309.
24. Rosinski J, et al. (1988) Ice-forming nuclei in air masses over the Gulf of Mexico. *J Aerosol Sci* 19(5):539–551.
25. Schnell RC (1977) Ice nuclei in seawater, fog water and marine air off the coast of Nova Scotia: Summer 1975. *J Atmos Sci* 34(8):1299–1305.
26. Schnell RC, Vali G (1975) Freezing nuclei in marine waters. *Tellus* 27(3):321–323.
27. Knopf DA, Alpert PA, Wang B, Aller JY (2011) Stimulation of ice nucleation by marine diatoms. *Nat Geosci* 4(2):88–90.
28. Wilson TW, et al. (2015) A marine biogenic source of atmospheric ice-nucleating particles. *Nature* 525(7568):234–238.

29. Trenberth KE, Fasullo JT (2010) Simulation of present-day and twenty-first-century energy budgets of the Southern Oceans. *J Clim* 23(2):440–454.

30. Morrison AE, Siems ST, Manton MJ (2011) A three-year climatology of cloud-top phase over the Southern Ocean and North Pacific. *J Clim* 24(9):2405–2418.

31. Huang Y, Siems ST, Manton MJ, Protat A, Delanoë J (2012) A study on the low-altitude clouds over the Southern Ocean using the DARDAR-MASK. *J Geophys Res* 117(D18):D18204.

32. Stanfield R, et al. (2014) Assessment of NASA GISS CMIP5 and post-CMIP5 simulated clouds and TOA radiation budgets using satellite observations: Part I: Cloud fraction and properties. *J Clim* 27(11):4189–4208.

33. Kanitz T, et al. (2011) Contrasting the impact of aerosols at northern and southern midlatitudes on heterogeneous ice formation. *Geophys Res Lett* 38(17):L17802.

34. Chubb TH, Jensen JB, Siems ST, Manton MJ (2013) In situ observations of supercooled liquid clouds over the Southern Ocean during the HIAPER Pole-to-Pole Observation campaigns. *Geophys Res Lett* 40(19):5280–5285.

35. Grosvenor DP, et al. (2012) In-situ aircraft observations of ice concentrations within clouds over the Antarctic Peninsula and Larsen Ice Shelf. *Atmos Chem Phys* 12(21):11275–11294.

36. Bromwich DH, et al. (2012) Tropospheric clouds in Antarctica. *Rev Geophys* 50(4):RG1004/2012.

37. Prather KA, et al. (2013) Bringing the ocean into the laboratory to probe the chemical complexity of sea spray aerosol. *Proc Natl Acad Sci USA* 110(19):7550–7555.

38. Stokes MD, et al. (2013) A marine aerosol reference tank system as a breaking wave analogue for the production of foam and sea-spray aerosols. *Atmos Meas Tech* 6(4):1085–1094.

39. Collins DB, et al. (2014) Direct aerosol chemical composition measurements to evaluate the physicochemical differences between controlled sea spray aerosol generation schemes. *Atmos Meas Tech* 7(11):3667–3683.

40. Heintzenberg J, Covert DC, Van Dingenen R (2000) Size distribution and chemical composition of marine aerosols: A compilation and review. *Tellus* 52B(4):1104–1122.

41. Garcia E, et al. (2012) Biogenic ice nuclei in boundary layer air over two U.S. High Plains agricultural regions. *J Geophys Res* 117(D18):D18209.

42. Wang X, et al. (2015) Microbial control of sea spray aerosol composition: A tale of two blooms. *ACS Cent Sci* 1(3):124–131.

43. Murray BJ, O'Sullivan D, Atkinson JD, Webb ME (2012) Ice nucleation by particles immersed in supercooled cloud droplets. *Chem Soc Rev* 41(19):6519–6554.

44. Quinn PK, Collins DB, Grassian VH, Prather KA, Bates TS (2015) Chemistry and related properties of freshly emitted sea spray aerosol. *Chem Rev* 115(10):4383–4399.

45. Heymsfield A, Willis P (2014) Cloud conditions favoring secondary ice particle production in tropical maritime convection. *J Atmos Sci* 71(12):4500–4526.

46. Lawson RP, Woods S, Morrison H (2015) The microphysics of ice and precipitation development in tropical cumulus clouds. *J Atmos Sci* 72(6):2429–2445.

47. Lewis ER, Teixeira J (2015) Dispelling clouds of uncertainty. *EOS* 96(12):16–19.

48. Rogers DC (1988) Development of a continuous flow thermal gradient diffusion chamber for ice nucleation studies. *Atmos Res* 22(2):149–181.

49. Rogers DC, DeMott PJ, Kreidenweis SM, Chen Y (2001) A continuous flow diffusion chamber for airborne measurements of ice nuclei. *J Atmos Ocean Technol* 18(5):725–741.

50. Eidhammer T, et al. (2010) Ice initiation by aerosol particles: Measured and predicted ice nuclei concentrations versus measured ice crystal concentrations in an orographic wave cloud. *J Atmos Sci* 67(8):2417–2436.

51. Prenni AJ, et al. (2009) Ice nuclei characteristics from M-PACE and their relation to ice formation in clouds. *Tellus* 61B(2):436–448.

52. Hill TCJ, Georgakopoulos DG, DeMott PJ, Stump WL, Franc GD (2014) Measurement of ice nucleation-active bacteria on plants and in precipitation by quantitative PCR. *Appl Environ Microbiol* 80(4):1256–1267.

53. Hiranuma N, et al. (2015) A comprehensive laboratory study on the immersion freezing behavior of illite NX particles: A comparison of 17 ice nucleation measurement techniques. *Atmos Chem Phys* 15(5):2489–2518.

54. Spurny KR, Lodge JP, Jr (1972) Collection efficiency tables—for membrane filters used in the sampling and analysis of aerosols and hydrosols. *NCAR Technical Note* (National Center for Atmospheric Research, Boulder, CO), NCAR-TN/STR-77, Vol I.

55. Vali G (1971) Quantitative evaluation of experimental results on the heterogeneous freezing nucleation of supercooled liquids. *J Atmos Sci* 28(3):402–409.

56. Agresti A, Coull BA (1998) Approximate is better than "exact" for interval estimation of binomial proportions. *Am Stat* 52(2):119–126.

57. Mason RH, et al. (2015) The micro-orifice uniform deposit impactor-droplet freezing technique (MOUDI-DFT) for measuring concentrations of ice nucleating particles as a function of size: Improvements and initial validation. *Atmos Meas Tech* 8(7):2449–2462.

58. Marple VA, Willeke K (1976) Impactor design. *Atmos Environ* 10(6):891–896.

59. Koop T, Luo B, Biermann UM, Crutzen PJ, Peter T (1997) Freezing of $HNO_3/H_2SO_4/H_2O$ solutions at stratospheric temperatures: Nucleation statistics and experiments. *J Phys Chem A* 101(6):1117–1133.

60. Ming Y, Russell L (2001) Predicted hygroscopic growth of sea salt aerosol. *J Geophys Res* 106(D22):28259–28274.

61. Snider JR, Petters MD (2008) Optical particle counter measurement of marine aerosol hygroscopic growth. *Atmos Chem Phys* 8(7):1949–1962.

62. Strapp JW, Leaitch WR, Liu PSK (1992) Hydrated and dried aerosol-size-distribution measurements from Particle Measuring Systems FSSP-300 probe and deiced PCASP-100X probe. *J Atmos Ocean Technol* 9(5):548–555.

63. Petters MD, Kreidenweis SM (2007) A single parameter representation of hygroscopic growth and cloud condensation nucleus activity. *Atmos Chem Phys* 7(8):1961–1971.

64. Craig L, et al. (2013) Characterizations of cloud droplet shatter artifacts in two airborne aerosol inlets. *Aerosol Sci Technol* 47(6):662–671.